JOURNAL OF MATERIALS SCIENCE 19 (1984) 1029–1042

A diffusion model for the oxidation of hot pressed Si_3N_4–Y_2O_3–SiO_2 materials

G. N. BABINI, A. BELLOSI, P. VINCENZINI
CNR, Research Institute for Ceramics Technology, Faenza, Italy

The parabolic oxidation behaviour of silicon nitride hot pressed from compositions of the Si_3N_4–Si_2N_2O–$Y_2Si_2O_7$ subsystem studied in 98 kPa air and 1273 to 1673 K has been discussed in terms of a diffusion model in which the most relevant parameters are the amount of the grain boundary phase, the width of the diffusion zone and the concentration gradient at the Si_3N_4/oxide reaction interface. The model accounts for both kinetic (oxidation rate constants) and thermodynamic (apparent activation energy for oxidation) variations with amount and composition of the grain boundary phase and proves suitable for the extension to other additive systems. The apparent activation energy for oxidation ranged from 260 to 623 kJ mol^{-1} according to composition. It is suggested that a more appropriate evaluation of the thermodynamic parameters of the diffusion process must account for the variation of concentration profiles of the diffusing species with temperature.

1. Introduction

Most of the studies on the oxidation of hot pressed silicon nitride (HPSN) stress the decisive role of transport phenomena in the bulk of the material. Diffusion of additive and impurities within the grain boundary phase has been generally suggested [1–5] as the rate governing step for the parabolic oxidation behaviour observed in a range of testing conditions. However, a satisfactory understanding of the specific influence of the characteristics of the grain boundary phase on diffusion, and hence on oxidation, has not yet been achieved. Oxidation kinetics have been discussed in terms of the amount of additive [5–11], occurrence of easy-to-oxidize phases such as in the Si_3N_4–Si_2N_2O–$Y_2Si_2O_7$ subsystem [6, 10, 12], and viscosity of the grain boundary phase [13]. Thermodynamic considerations also dictate that both product and rate of oxidation depend on the initial material composition [14]. This study is an attempt to discuss oxidation data of selected compositions in the Si_3N_4–Y_2O_3–SiO_2 system in terms of specific parameters of the material which enter into the diffusion equations, such as concentration gradient of diffusing species and geometry of the diffusion path. Although the complexity of the material requires the use of a number of simplifying assumptions, the model accounts for some kinetic and thermodynamic aspects of oxidation of HPSN in the Si_3N_4–Y_2O_3–SiO_2 system. Its use can be satisfactorily extended to other additive systems.

2. Experimental details

2.1. Materials

Twelve Si_3N_4–Y_2O_3–SiO_2 compositions belonging to the oxidation resistant Si_3N_4–Si_2N_2O–$Y_2Si_2O_7$ compatibility triangle (Fig. 1)* were uniaxially hot pressed at 1973 K and 34.3 MPa in 98 kPa nitrogen atmosphere to nearly full density. Batches were prepared from commercial

*Points on Fig. 1 represent normal compositions of the starting batches. The final composition of the hot pressed materials is shifted as a consequence of Si_3N_4 volatilization during hot pressing. Therefore crystal phases other than those predictable on the basis of the Si_3N_4–Si_2N_2O–$Y_2Si_2O_7$ compatibility triangle can be found due also to the presence of impurities of metal cations.

0022–2461/84 $03.00 + .12

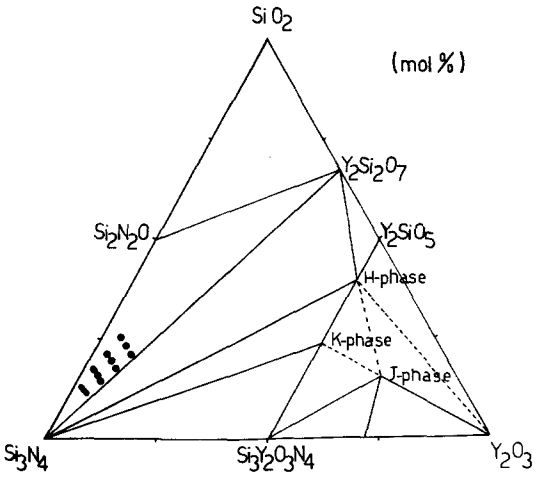

Figure 1 Si_3N_4–Y_2O_3–SiO_2 equilibrium diagram. Compositions investigated in the Si_3N_4–Si_2N_2O–$Y_2Si_2O_7$ compatibility triangle are shown.

grade Si_3N_4[†] and reagent grade SiO_2 and Y_2O_3, by wet mixing in isobutyl alcohol in a plastic jar with alumina balls for 72 h. The above compositions were selected to form three groups characterized by a similar but not exactly equal SiO_2/Y_2O_3 ratio. The notation xYz has been adopted in which $x = 1$ to 4 represents the Si_3N_4 content and $z = 2, 3, 5$ stands for the appropriate SiO_2/Y_2O_3 ratio. Table I collects the sample compositions on the assumption that all surface silica and impurities become silicates.

SEM micrographs (Fig. 2) of the hot pressed materials show a mean size of 1 μm for the Si_3N_4 grains. The secondary phase wets the grain boundaries and is also present on occasion in the form of discrete particles easily detected by WDS[‡] mapping. Different crystal phases including yttrialite $(H, Na, F)_5(Y, La)_5Si_6O_{21}$ and miserite (Ca, K, Na, Al, Y) SiO_3 solid solutions, silicon oxynitride Si_2N_2O, different species of yttrium silicates (δ- and z-$Y_2Si_2O_7$, $Y_{4.67}(SiO_4)_3O$) and possibly also yttrium silicon oxynitride $Y_5(SiO_4)_3N$ shown by X-ray diffraction analysis are the main crystalline constituents of the secondary phase, their presence and relative amounts being dependent on composition. Upon reheating at 1573 K for different soaking times, further recrystallization of secondary phases occurs accompanied by some reconstructive transformation which cause more yttrialite and miserite and significant amounts of $Y_2Si_2O_7$ to form.

The evaluation of residual porosity in the hot pressed materials, which has been observed to affect oxidation at relatively low temperature, requires a theoretical density for each composition that can be calculated on the following assumptions as regards the volumetric composition[§] of the intergranular phase:

(i) at the hot pressing temperature, all Y_2O_3 combines with SiO_2 to form yttrium silicates ($Y_2Si_2O_7$ and/or $Y_4Si_3O_{12}$) according to the equilibrium diagram of the Y_2O_3–SiO_2 binary (Fig. 3);

(ii) all residual SiO_2 reacts with silicon nitride to silicon oxynitride. (This assumption in reality does not affect the theoretical density since the Si_2N_2O density is exactly the mean of those of SiO_2 and Si_3N_4);

(iii) all metal impurities are present in the silicate phases.

TABLE I Starting batches of the investigated Si_3N_4–Y_2O_3–SiO_2 compositions

	1Y2	2Y2	3Y2	4Y2	1Y3	2Y3	3Y3	4Y3	1Y5	2Y5	3Y5	4Y5
Si_3N_4 (mol%)	72.07	77.33	82.64	88.08	72.05	77.32	82.63	88.04	72.08	77.32	82.65	88.02
SiO_2* (mol%)	17.44	13.85	10.23	6.50	19.72	15.69	11.62	7.46	21.98	17.52	12.97	8.40
Y_2O_3 (mol%)	9.08	7.30	5.51	3.69	6.81	5.47	4.13	2.77	4.52	3.65	2.76	1.84
Impurities (computed as silicates)	1.42	1.52	1.63	1.73	1.42	1.52	1.63	1.73	1.42	1.52	1.63	1.73
SiO_2/Y_2O_3 (molar ratio)	1.92	1.90	1.86	1.76	2.90	2.87	2.81	2.69	4.86	4.80	4.70	4.57

*Includes the SiO_2 contained in the Si_3N_4 powder.

†AME-Refractory Grade. BET specific surface area 3.72 $m^2\ g^{-1}$; amorphous SiO_2 1.9 wt%; Si (metal) 1.4 wt%; Chemical analysis: Si (total) 58.41%; N 37.73%; Al 0.42%; Fe 0.46%; Ca 0.13%; Mg 220 ppm; Na 120 ppm; K < 50 ppm; α/β ratio 3.8 (volumetric).

‡WDS = Wavelength Dispersion Spectrometer.

§The need is not to specify the exact composition of the grain boundary phase but to define its fraction volume in the material which is an appropriate parameter for the oxidation model which will be introduced in Section 4.

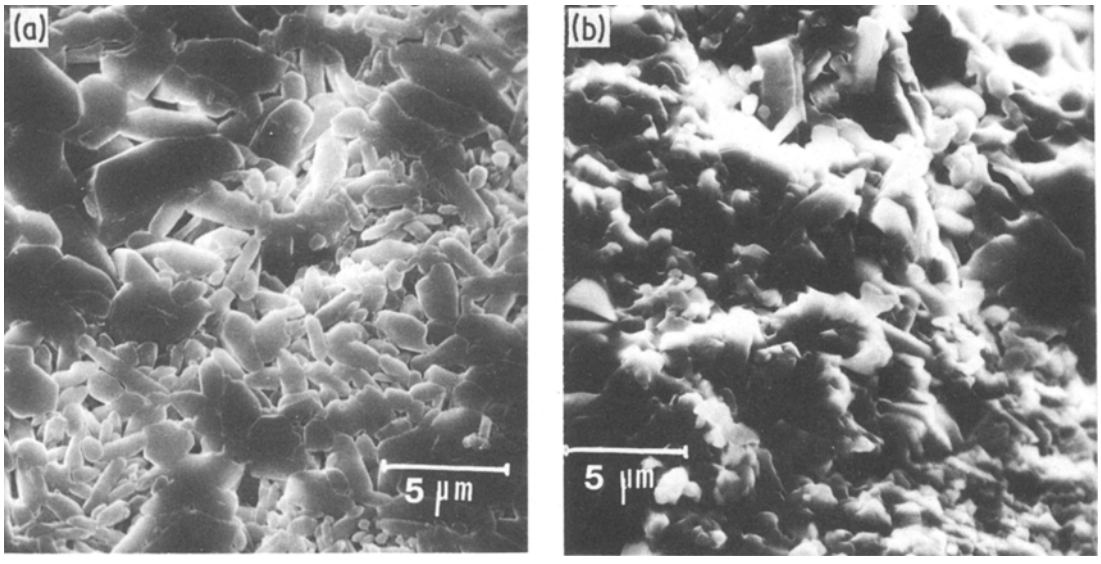

Figure 2 Scanning electron micrographs of HPSN doped with 6.9 wt% Y_2O_3–5.2%SiO_2 (a) polished and etched surface (molten NaOH, 20 sec); (b) fracture surface.

Table II collects results of this analysis. Table III compares the calculated and experimental densities. The resulting residual porosity is in quite good agreement with the SEM evaluations for samples xY5 and xY2. For samples xY3 it was necessary to assume a grain boundary composition similar to set xY2 to have a similar agreement. This assumption is quite reasonable due to the low-melting cation impurities which shift the xY3 composition (nominally approaching the SiO_2–Y_2O_3 eutectic) to $2Y_2O_3 \cdot 3SiO_2$ corresponding to xY2.

2.2. Oxidation tests

The oxidation experiments were carried out in 98 kPa air atmosphere on square samples (10 by 10 by 2 mm) diamond cut from the hot pressed billetts, wet-polished with various grades of diamond paste up to 1 μm, and ultrasonically cleaned in acetone. Weight gain was continuously recorded by using a TG apparatus* capable of 20 μg resolution. Oxidation temperatures ranged from 1173 to 1673 K; the heating and cooling rates were 20 and 10 K min^{-1}, respectively. A nearly constant oxidation time of 30 h was main-

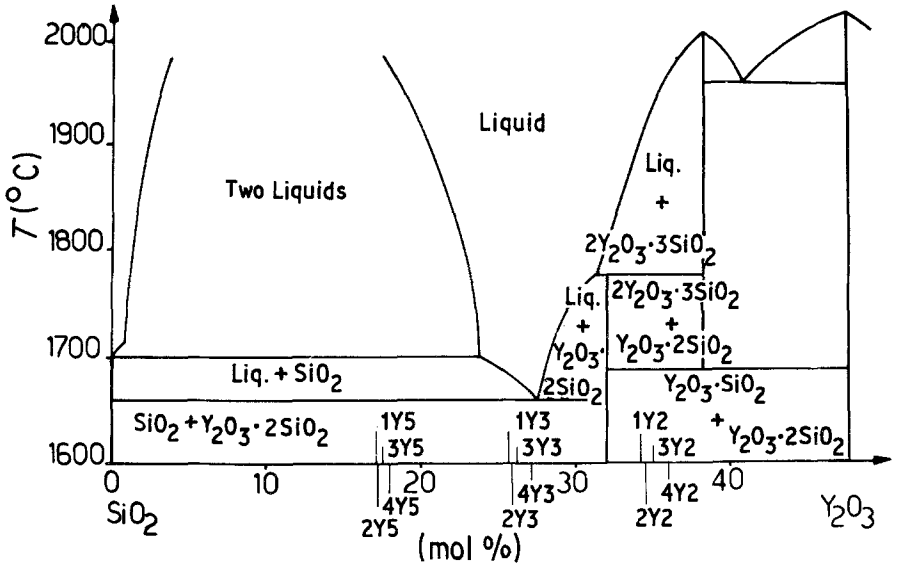

Figure 3 Location of the twelve compositions studied on the SiO_2–Y_2O_3 binary according to the SiO_2/Y_2O_3 ratio.

*Netzsch Geratebau, Selb, Federal Republic of Germany.

TABLE II Theoretical compositions of the hot pressed samples (mol%) and grain boundary width calculated on the assumption of cubic particles of 1 μm size

	1Y2	2Y2	3Y2	4Y2	1Y3	2Y3	3Y3	4Y3	1Y5	2Y5	3Y5	4Y5
Si_3N_4	85.23	88.58	91.69	94.72	73.72	79.44	84.90	90.19	65.02	72.38	79.59	86.49
$Y_2O_3 \cdot 2SiO_2$	3.70	2.85	2.06	1.33	2.63	2.05	1.50	0.98	4.97	3.94	2.92	1.91
Si_2N_2O	5.64	3.94	2.35	0.76	19.38	14.76	10.33	6.02	28.45	22.05	15.77	9.80
Impurities	1.74	1.78	1.83	1.87	1.64	1.71	1.78	1.83	1.56	1.64	1.73	1.80
$2Y_2O_3 \cdot 3SiO_2$	3.70	2.85	2.06	1.33	2.63	2.05	1.50	0.98	–	–	–	–
Silicates	9.14	7.48	5.95	4.53	6.90	5.81	4.78	3.79	6.33	5.58	4.65	3.71
Grain boundary width (μm)												
Silicates	0.076	0.060	0.045	0.032	0.057	0.046	0.035	0.025	0.041	0.033	0.026	0.019
Total	0.095	0.073	0.052	0.034	0.127	0.095	0.068	0.043	0.150	0.111	0.078	0.049

TABLE III Theoretical, experimental and relative density of the hot pressed samples

Sample	Evaluated theoretical density ($g\ cm^{-3}$)	Measured density ($g\ cm^{-3}$)	Relative density (%)
1Y2	3.366	3.30	0.98
2Y2	3.330	3.26	0.98
3Y2	3.295	3.295	1.00
4Y2	3.261	3.16	0.97
1Y3	3.283	3.23	0.98
2Y3	3.264	3.22	0.99
3Y3	3.246	3.25	1.00
4Y3	3.229	3.15	0.98
1Y5	3.199	3.17	0.99
2Y5	3.199	3.18	0.99
3Y5	3.198	3.21	1.00
4Y5	3.197	3.14	0.98

tained for all experiments. Additional runs up to 100 h were also performed on some samples. Before and after oxidation, the samples were weighed to ± 10 μg.

Surfaces and cross-sections of the oxide scales were analysed by XRD†, SEM‡, including back-scattered electron imagining, WDS (Wavelength Dispersion System)§ and EDS (Energy Dispersion System)¶.

3. Results

3.1. Oxidation kinetics

The weight gain against time curves for (Y_2O_3 + SiO_2)-doped HPSN oxidized in static air at 1273 to 1673 K approximate to the classical parabolic behaviour represented by the equation:

$$W^2 = Kt + b \cong Kt \qquad (1)$$

where $W = \Delta W/s$ is the weight gain ($mg\ cm^{-2}$) at time t, $K = K_0 \exp(-E_a/RT)$ ($mg^2\ cm^{-4}\ min^{-1}$) is the parabolic rate constant and b is a constant which accounts for the effect of a possible non-parabolic initial stage, i.e. for the uncertainty of the exact definition of the beginning ($t = 0$) of the parabolic process. Only in a few cases, and at low oxidation temperatures (below ~1323 K) non-parabolic oxidation kinetics were observed for some samples, this possibly being related to residual porosity and/or the occurrence of easily oxidizable yttrium oxynitrides. Plots of W^2 as a function of time are reported in Figs. 4 and 5 for samples 1Y5 and 4Y5–4Y2, respectively.

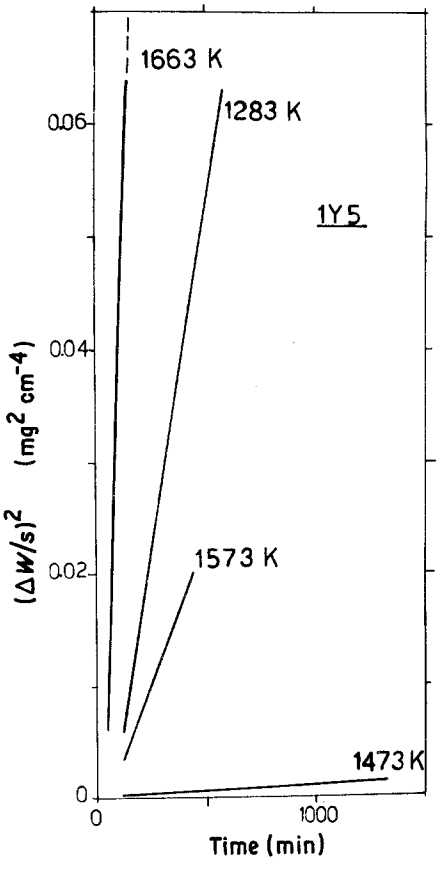

Figure 4 Parabolic weight gain for sample 1Y5 oxidized at 98 kPa in air.

The parabolic rate constants, K, for oxidation of Si_3N_4, determined from a mathematical interpolation of the isothermal weight gain curves and reported as a function of temperature in Arrhenius plots, result in apparent activation energies for oxidation varying from 260 kJ mol^{-1} to 623 kJ mol^{-1} at $T = 1423$ to 1673 K, according to composition. Values somewhat lower are obtained by using the oxidation rate constants derived by weighing the samples before and after the oxidation run and assuming parabolic kinetics, this being possibly related to the weight gain which occurs during the heating-up time of the oxidation temperature. The large variation of E_a with composition within materials belonging to the same system is unusual. In MgO-doped HPSN E_a varies

†D 500, Siemens AG, Karlsruhe, Federal Republic of Germany.
‡Autoscan, Etec Corp., Hayward, Cal., USA.
§Autospec, Etec Corp., Hayward, Cal., USA.
¶EDAX PV9100-EDAX Int. Corp., Ill., USA.

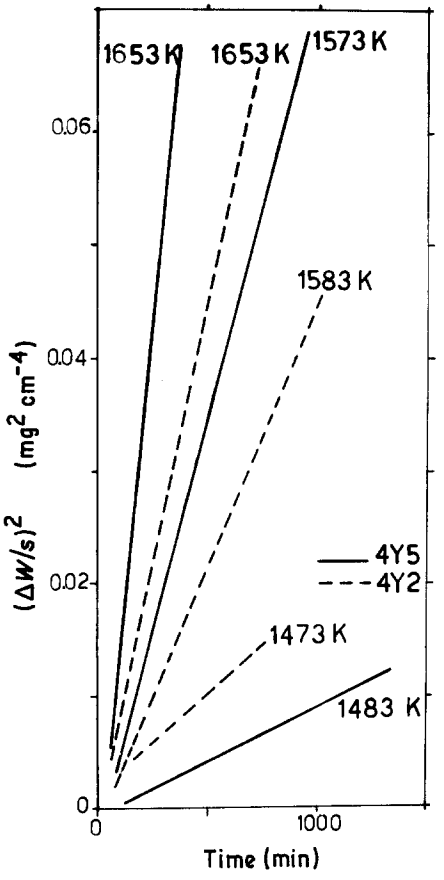

Figure 5 Parabolic weight gain for samples 4Y2 and 4Y5 oxidized at 98 kPa in air.

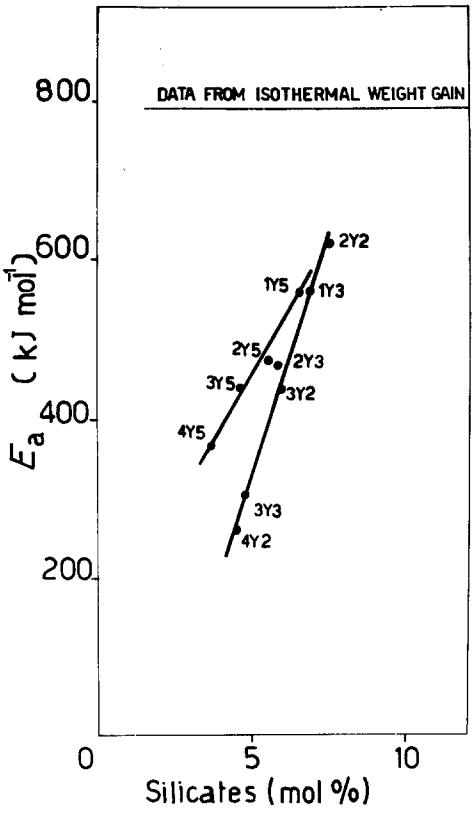

Figure 6 Relation among the apparent activation energy for oxidation and the content in silicates of the intergranular phase: data from isothermal weight gain.

in a relatively narrow range (378 to 488 kJ mol^{-1}) irrespective of the oxidation conditions [1, 8, 15], although K values prove sensitive to both oxidation atmosphere and material composition, and are practically unaffected by the amount of sintering aid. Materials hot pressed from the Si_3N_4–CeO_2 system [5] also resulted in almost constant E_a values of 385 to 400 kJ mol^{-1} at $T = 1373$ to 1623 K for CeO_2 contents from 2.5 to 20 wt%. The introduction of some amount of SiO_2 in the starting mix lowered this value to ~ 350 kJ mol^{-1}. The only literature source for Y_2O_3-doped HPSN gives $E_a = 450$ kJ mol^{-1} at $T < 1700$ K, for a commercial product* oxidized at 1620 to 1796 K in 20 kPa oxygen.

A plot of E_a against mol% silicates in the hot pressed samples (Fig. 6) results in linear relationships. Data points fit two different straight lines for xY2–xY3 and xY5 compositions. Amount, composition and structure of the secondary phase and residual porosity are the main parameters of the materials which affect K and E_a at given oxidation conditions. It is worth pointing out that we are confined here only to the less relevant changes deriving from variations in amount and composition within a specific system. The one or more order of magnitude differences in the oxidation rate constants at "homologous" temperatures between different systems are mostly to be related to the general properties of the grain boundary phase, i.e. to viscosity which had been shown to strongly affect oxidation rates.

Plots of isothermal K values at 1573 K, against Y_2O_3 and SiO_2 contents in the starting batch and against the overall amount of intergranular phase in the hot pressed samples are reported in Figs. 7, 8 and 9, respectively. The best account for kinetic (K) and thermodynamic (E_a) data is given by Fig. 9. The distinct variation for the xY5 and xY2–xY3 materials also agrees with results in Fig. 6.

Compositions 1Y2 and 1Y5 are relevant exceptions to the general trend; a different approach is

*NC X34, Norton, Mass, USA.

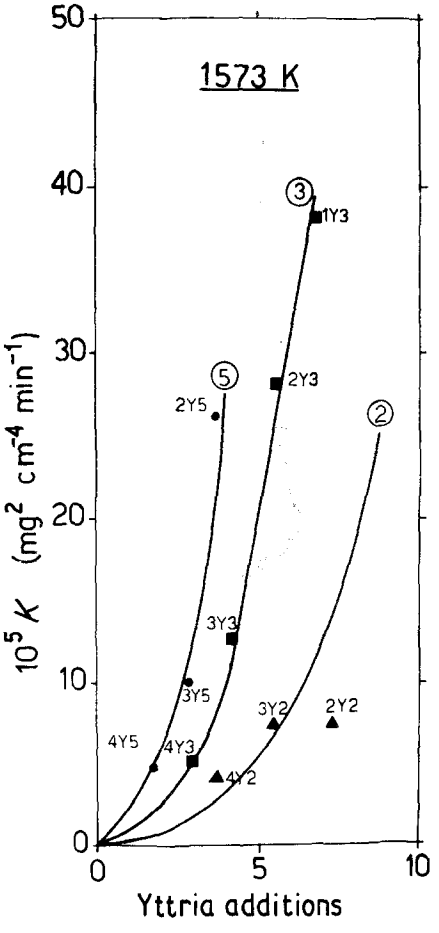

Figure 7 Oxidation rate constants at 1573 K as a function of yttria content in the starting mix.

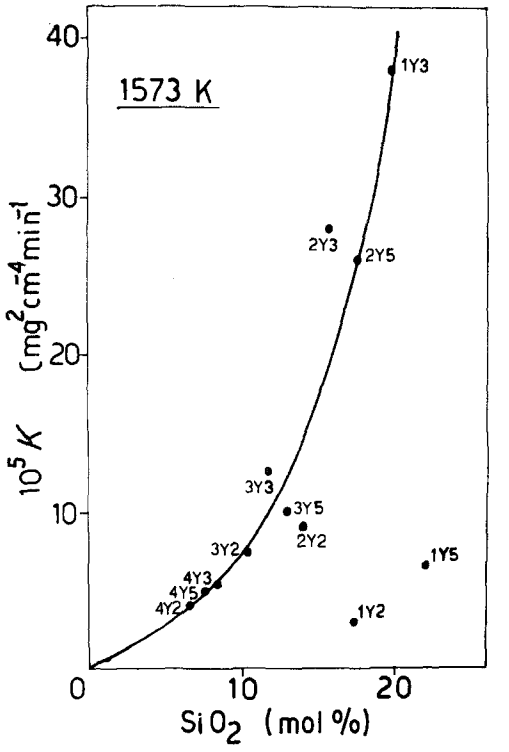

Figure 8 Oxidation rate constants at 1573 K as a function of silica content in the starting mix.

therefore needed to achieve a more satisfactory explanation of the oxidation behaviour of this class of materials (see Section 4).

3.2. Morphology of the oxide scales

Composition, structure and morphology of the oxide layer on HPSN depend both on oxidation conditions and material characteristics. Oxide scales having very different type and amount of oxidized crystalline, pseudo-amorphous or glassy products result from oxidation of materials at different Y_2O_3/SiO_2 ratios, time and temperature.

In oxidizing conditions where the oxide layer is non-protective, the overall characteristics of the outer oxide scales exert but a secondary role on oxidation. Thus only a few examples of the varied morphology of oxidized samples surfaces after 30 and 100 h exposure at 1573 K, where the main oxidation products are yttrium silicates, especially $Y_2Si_2O_7$, and cristobalite are shown (Fig. 10). Yttria dendrites also result from edge dissolution of yttrium silicates and reprecipitation from the glassy phase containing most of the metal cation impurities that diffused to the oxide scale. The amount of yttrium silicate crystals in the oxide layer is evidence of the large contri-

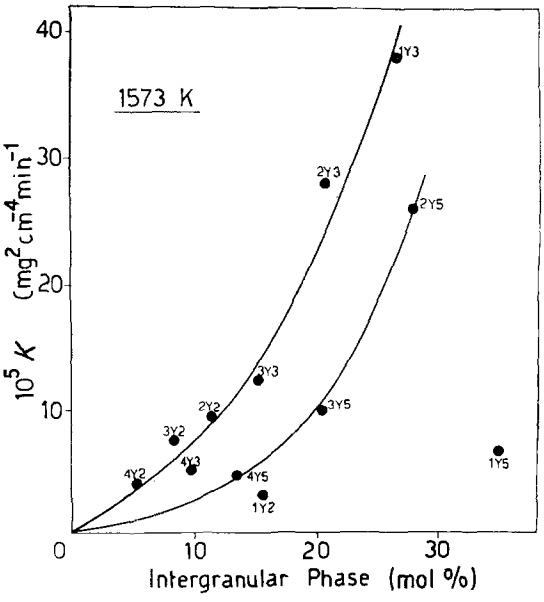

Figure 9 Oxidation rate constants at 1573 K as a function of the overall amount of the intergranular phase.

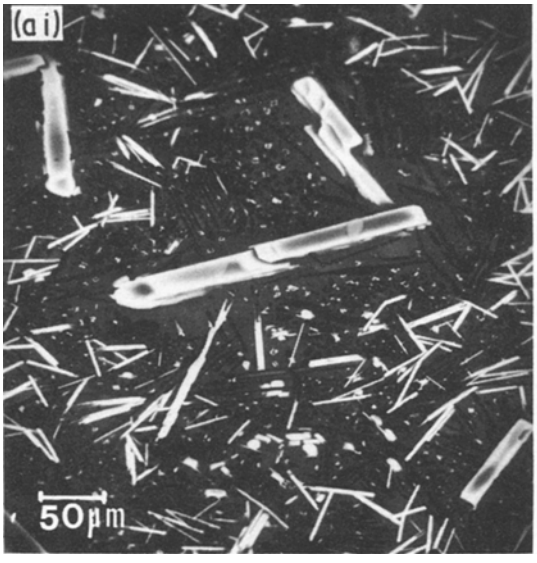

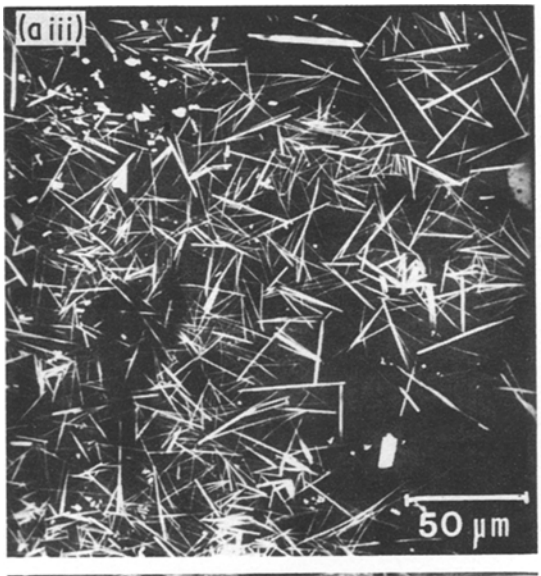

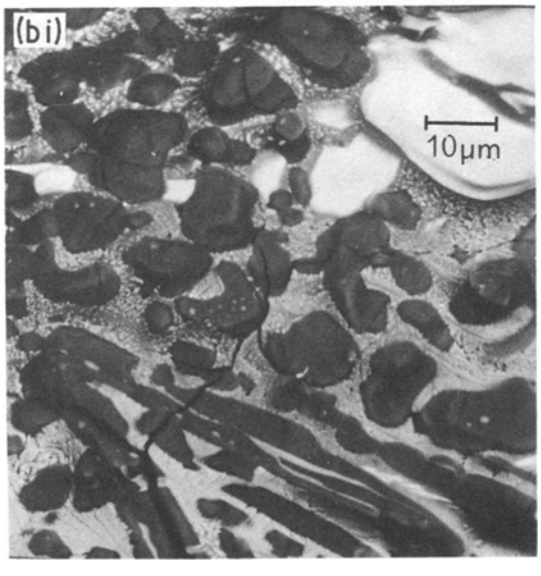

Figure 10 (a) SEM micrograph (backscattered electron images) of HPSN sample in the $Si_3N_4-Y_2O_3-SiO_2$ system, oxidized at 1573 K for 30 h: (i) 3Y2 (9.1 wt% Y_2O_3 + 4.5 wt% SiO_2); (ii) 3Y3 (6.9 wt% Y_2O_3 + 5.2 wt% SiO_2); (iii) 3Y5 (4.7 wt% Y_2O_3 + 5.8 wt% SiO_2) Needle-like and plate-like $Y_2O_3 \cdot 2SiO_2$ crystals (white areas); needle-like or lenticular SiO_2 (cristobalite) forms (dark areas); silica rich glassy (amorphous) phase bearing large amounts of impurity and additive atoms (grey areas). (b) SEM micrographs (backscattered electron images) of HPSN samples in the $Si_3N_4-Y_2O_3-SiO_2$ system, oxidized at 1653 K for 30 h: (i) 2Y2 (12.1 wt% Y_2O_3 + 6.1 wt% SiO_2); (ii) 3Y2 (9.1 wt% Y_2O_3 + 4.5 wt% SiO_2); (iii) 4Y2 (6.0 wt% Y_2O_3 + 2.8 wt% SiO_2). (i) Plate-like crystals of yttrium silicates (white areas) showing partial dissolution in the silica-rich amorphous (glassy) phase and incipient reprecipitation of Y_2O_3 dendrites during cooling; SiO_2 (cristobalite) crystal forms (dark areas); (ii) Plate-like $Y_2O_3 \cdot 2SiO_2$ crystals embedded in the amorphous (glassy) silica rich phase, (iii) Plate-like $Y_2O_3 \cdot 2SiO_2$ crystals (white areas); lenticular SiO_2 (cristobalite) forms (dark areas); silica rich amorphous (glassy) phase (grey areas). (c) SEM micrographs (backscattered electron images) of HPSN samples of the $Si_3N_4-Y_2O_3-SiO_2$ system, oxidized at 1573 for 100 h: (i) 2Y2 (12.1 wt% Y_2O_3 + 6.1 wt% SiO_2); (ii) 3Y2 (9.1 wt% Y_2O_3 + 4.5 wt% SiO_2); (iii) 4Y2 (6.0 wt% Y_2O_3 + 2.8 wt% SiO_2). (i) $Y_2O_3 \cdot 2SiO_2$ mainly in plate-like form (white areas) showing partial dissolution and dendritic $Y_2O_3 \cdot 2SiO_2$ precipitates in the silica-rich glassy phase (grey areas) bearing also needle-like and lenticular SiO_2 (cristobalite) crystals (dark areas); (ii) Granular and needle-like $Y_2O_3 \cdot 2SiO_2$ crystals embedded in the silica-rich amorphous (glassy) phase; (iii) $Y_2O_3 \cdot 2SiO_2$ granular and elongated crystals (white areas) embedded in the silica-rich amorphous (glassy) phase (grey areas) bearing needle-like and lenticular SiO_2 (cristobalite) forms (dark areas).

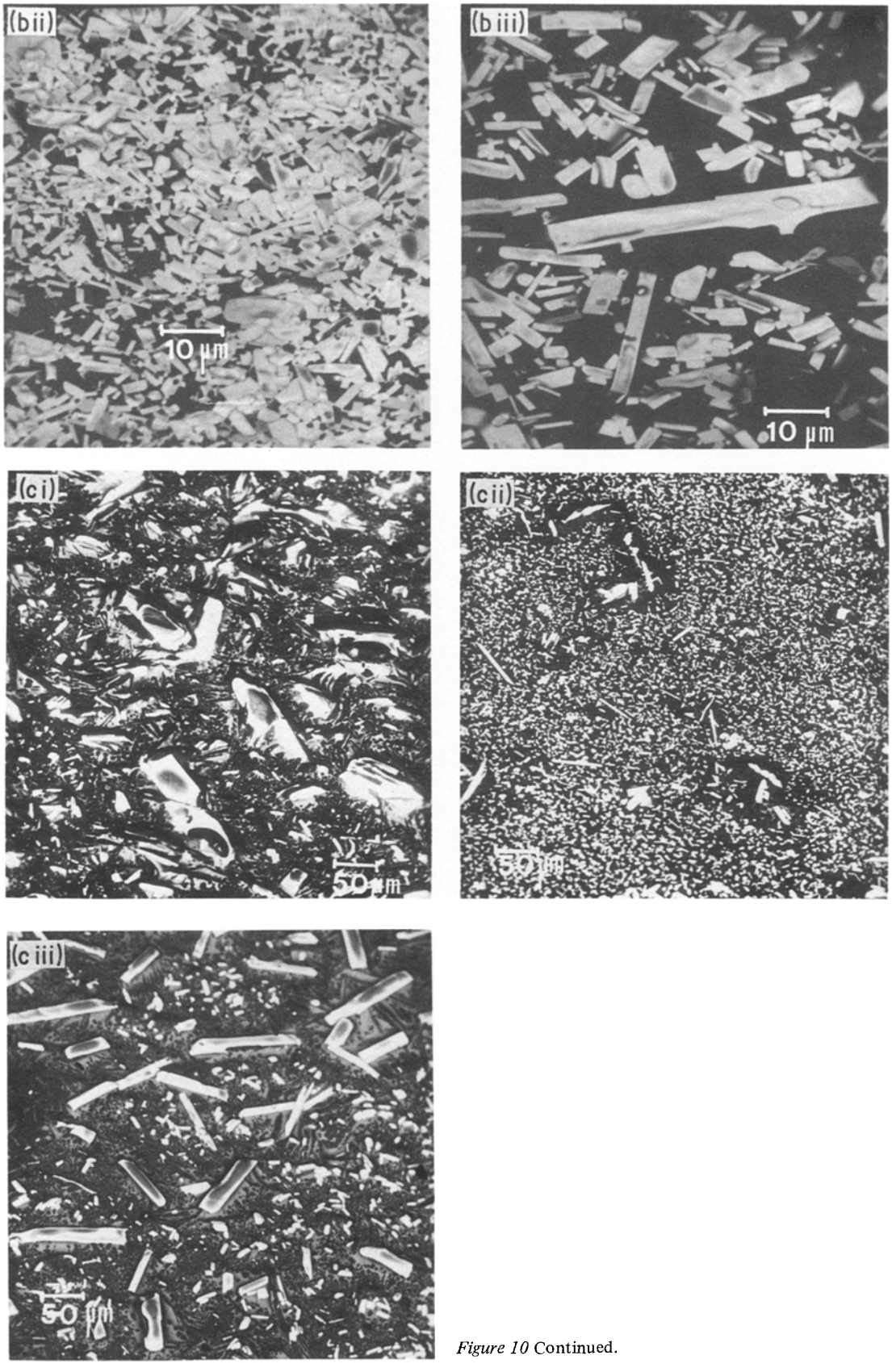

Figure 10 Continued.

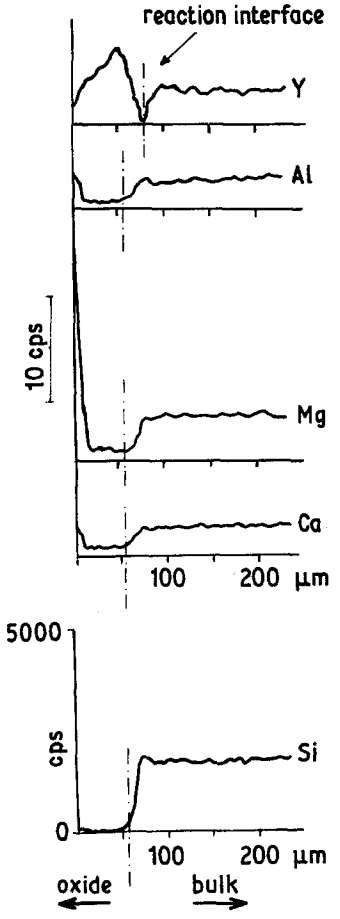

Figure 11 EDS profiles of silicon and metallic cations in the cross section of the sample 2Y3 oxidized at 1573° C for 3 h.

bution to oxidation offered by yttrium diffusion from the bulk. Most important for discussing the phenomenology of the oxidation process of HPSN are the compositional shifts which occur at the interior of the hot pressed body and at the Si_3N_4/oxide reaction interface [1–5]. Fig. 11 shows the qualitative EDS diffusion profiles of yttrium, calcium, magnesium and aluminium observed on a fracture cross-section of sample 2Y3 oxidized at 1573 K for 30 h. Two independent concentration gradients are established, the first between the bulk and the reaction interface, the other inside the oxide layer, the minimum metal cation concentration occurring at the Si_3N_4/oxide interface. These results agree with previous observations in other HPSN systems [3, 6, 15].

4. Discussion

The analysis will be confined at temperatures from 1323 to 1623 K where the effect of residual porosity can be neglected and the same rate-governing mechanism can reasonably be suggested for all compositions. Parabolic kinetics and E_a values stand for a cation-diffusion controlled oxidation process. The close link between E_a and composition also suggests that diffusion is largely dominated, at a given temperature, by the characteristics of the grain boundary phase.

According also to previous findings [2–5], the rate controlling step of the oxidation process is assumed to be the diffusion of metal cations (additive and impurities) from the grain boundary phase through the Si_3N_4/oxide reaction interface to the oxide scale.

Thus the diffusion process can be tentatively described by Fick's 1st law:

$$J = -D\partial C/\partial x \qquad (2)$$

where J is the flux of the diffusion species, D is the diffusion coefficient pertaining to each diffusing species and C is the concentration at x (x, diffusion path).

The grain boundary phase is thought to consist of an assembly of equi-sized parallel channels of square cross-section having their axis aligned with the flow direction of the diffusing species (which is assumed to be perpendicular to the planar, infinite sized, reaction interface).

A further assumption necessary in order to apply Equation 2 to real systems, introduced only to simplify calculations, is a linear concentration gradient along the diffusion path, i.e.

$$\partial C/\partial x \cong (C_{gb} - C_{ri})/\Delta x = \frac{\Delta C}{\Delta x} \qquad (3)$$

where C_{gb} is the concentration in the grain boundary phase, C_{ri} is the concentration at the Si_3N_3/oxide reaction interface and Δx is the distance between the reaction interface and the unreacted material.

Points (i) to (iii) imply the following relation between ΔW and the flux J of metal cations:

$$\alpha\Delta W = JSt \qquad (4)$$

or

$$\alpha\frac{\Delta W}{t} = JS = -D\frac{dC}{dx}Na^2 \qquad (5)$$

where t is oxidation time, S is the total cross-section area of the diffusion channels, α is a proportionality constant, N is the number of diffusion channels for unit cross-section of the material and a^2 is the cross-section area of each channel. Since

$$\frac{\Delta W}{t} = \left(\frac{K}{t}\right)^{1/2}$$

$$\left(\frac{K}{t}\right)^{1/2} = \frac{D}{\alpha}\frac{N}{\Delta x}(C_{gb} - C_{ri})a^2 = Aa^2 \quad (6)$$

$$\frac{1}{a^2}\left(\frac{K}{t}\right)^{1/2} = \frac{D}{\alpha}\frac{N}{\Delta x}(C_{gb} - C_{ri}) = B\Delta C \quad (7)$$

where $N/\Delta x$ represents a geometrical factor which depends on time and on material.

Therefore, from Equations 6 and 7:

(i) when A = constant, i.e. Equation 6 is linear in a^2, it is likely that both C_{gb} and C_{ri} are constant at a given temperature with the amount of intergranular phase. Further since

$$K = f(A) \quad E_a = f(K) \rightarrow E_a = f(A) \quad (8)$$

an invariance of the apparent activation energy for oxidation on the amount of intergranular phase is to be expected.

(ii) when $A \neq$ constant, at least one parameter in A varies with the amount of intergranular phase. If B in Equation 7 is also constant, the changing parameter in A is the concentration gradient ΔC. Changes in E_a therefore do not necessarily require variations in other parameters such as D, $N/\Delta x$ or α.

Thus, in systems where the composition of the grain boundary phase is reasonably unaffected by the amount of sintering aid a constant E_a value is most probable. This conclusion has been verified to apply to Si_3N_4–MgO and Si_3N_4–CeO_2 systems.

In systems where variation in the composition of the grain boundary phase occurs as a result of increased amount of additive, as for the Si_3N_4–CeO_2–SiO_2 system [16] and the present Si_3N_4–Y_2O_3–SiO_2 materials, a variation of E_a with the amount of secondary phase is fully justified.

More than one single oxidation mechanism is most probably acting during oxidation in real system. Also if the direct reaction of Si_3N_4 with oxygen is neglected, it is likely that a number of different cation species are involved in the process, each contributing according to its amount and specific diffusion characteristics. Therefore all parameters in Equations 6 and 7 represent average values. Furthermore the variation of D as a function of the concentration profile along the diffusion path is not accounted for by the model. Finally the model requires the knowledge of the mean width of the grain boundary phase whose uncertainty is linked to both the simplifications introduced in the geometry of the diffusion channels and to the difficulty in assessing the exact material composition. This last point, however, does not affect calculations in this specific case, only relative values being involved.

In Fig. 12, Equation 6 is used to evaluate the oxidation data of Si_3N_4–Y_2O_3–SiO_2 samples. Due to the different composition, each sample is characterized by a different A value. The approximately regular change of A with the SiO_2/Y_2O_3 ratio and with the amount of Si_3N_3 in the materials shows evidence that at least one parameter in A varies with the above characteristics.

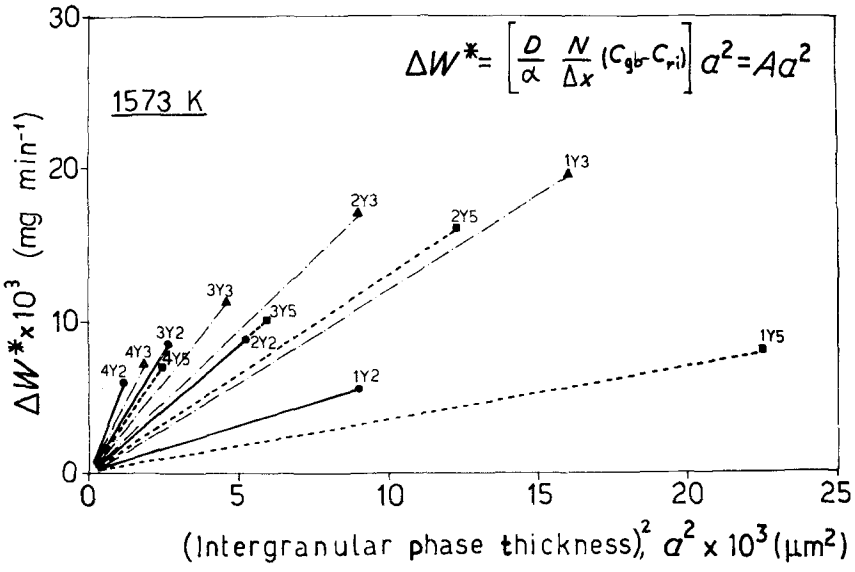

Figure 12 Application of Equation 6 to the experimental data at 1573 K.

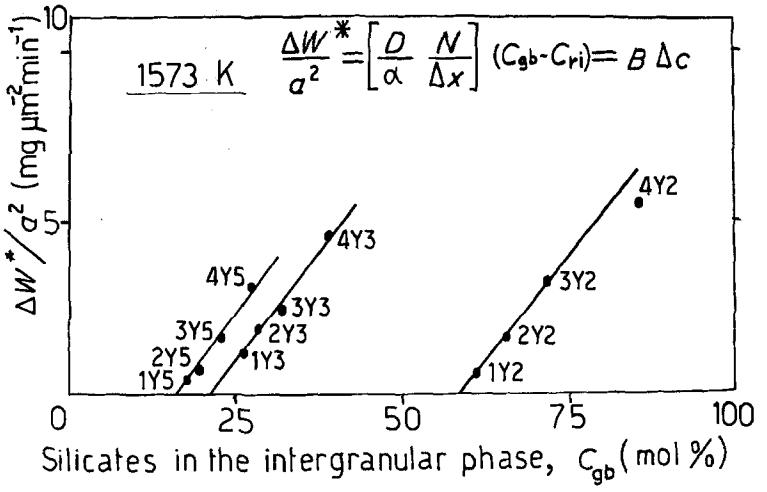

Figure 13 Application of Equation 7 to the experimental data at 1573 K.

Equation 7 can be used to assess if ΔC is such a parameter being ΔC dependent on both the SiO_2/Y_2O_3 ratio and on the Si_3N_4 fraction. The application of Equation 7 to the experimental data at 1573 K, represented in Fig. 13, gives three straight lines each corresponding to one of the xYz sets, with almost identical slopes, thus suggesting that the interface concentration C_{ri} depends on the SiO_2/Y_2O_3 ratio whereas all parameters which are included in B such as D, $N/\Delta x$ and, at a given temperature, are probably unaffected by the SiO_2/Y_2O_3 ratio and the amount of intergranular phase. Furthermore calculations show that C_{ri} is independent on time at a given oxidation temperature. The intercept of each of the straight lines on the abscisse ($\Delta W/a^2 = 0$) gives a point at which $C_{gb} = C_{ri}$, i.e. defines the composition of the grain boundary phase to which corresponds the maximum oxidation resistance of the material. Thus the model suggests a possible way to "build up" a material with optimum oxidation resistance for each operating temperature being both C_{gb} and C_{ri} (hence ΔC) independent on time during isothermal oxidation conditions.

Calculations of Equations 6 and 7 were performed at $t = 1$ min for sake of simplicity. The same conclusions as regards C_{ri} and apparent activation energy for diffusion would be attained at any other time.

By applying Equation 7 at a different temperature a similar behaviour is obtained. Fig. 14 represents data analysis at 1373 K. The factor of ten decrease of B, mainly related to the decrease of D with temperature, and the increase of equilibrium silicate concentration at the interface, which is possibly associated to less silica at disposal because of the lower oxidation rate, are the main deductions from this analysis.

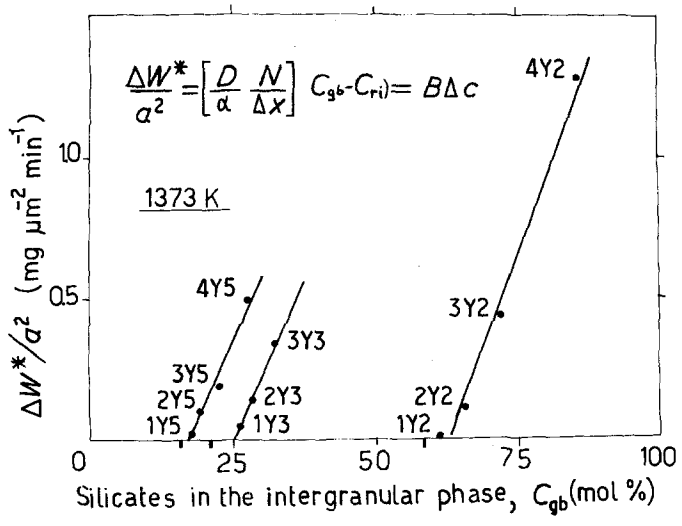

Figure 14 Application of Equation 7 to the experimental data at 1373 K.

An additional observation is that the interface concentration, and so the concentration gradient, depends on temperature which in turn through Equation 8 also effects E_a values. Extreme care is therefore needed when apparent activation energies derived from oxidation rate constants based on weight gain experiments are used to suggest possible diffusing species which govern oxidation. Equations 6 and 7 offer a chance for a more accurate estimation of the activation energy involved in the diffusion process. For a given material α, a^2 and N are nearly independent of temperature and Equation 6 and 7 can be rewritten as follows:

$$D = \frac{\alpha}{N}\frac{\Delta x}{\Delta C}A \doteqdot (\Delta C/\Delta x)^{-1}A \qquad (9)$$

$$D = \frac{\alpha}{N}\Delta xB \doteqdot \Delta xB \qquad (10)$$

Equation 9 requires the variation of both ΔC and Δx with temperature, whereas only the dependence of Δx is needed to evaluate D from Equation 10. Due to the complex microstructure of the material and the number of interacting diffusing cations a precise evaluation of the concentration gradient ΔC is very difficult. Therefore Equation 10 was used and applied to sample 2Y3. The same procedure can obviously be applied to all other compositions.

EDS elemental analysis of a fracture cross-section of 2Y3 oxidized at 1373, 1473 and 1573 K for 30 h results in $\Delta x = 10 \pm 2\,\mu m$, $\Delta x = 16 \pm 4\,\mu m$, and $\Delta x = 25 \pm 4\,\mu m$, respectively. The Arrhenius plot of the corresponding values obtained from Equation 10 give an average "true" activation energy for diffusion of $E_a = 240 \pm 20$ kJ mol^{-1}, i.e. a value substantially lower than the one obtained for the same sample by using the experimental oxidation rate constants (460 kJ mol^{-1}) and also those deriving from weight gain experiments on various HPSN materials [2–6, 8, 15].

The decrease of Δx with temperature, not accounted for by the previous studies, implies lower experimental K values at low temperatures (resulting in higher E_a) than those obtained if D were the only temperature-dependent parameter in Equations 6 and 7.

5. Conclusions

(i) Oxidation of $(Y_2O_3 + SiO_2)$-doped HPSN in 98 kPa air at 1273 to 1673 K results in parabolic kinetics and apparent activation energies for oxidation of 260 to 623 kJ mol^{-1}, depending on composition.

(ii) A diffusion model based on simple equations derived from Fick's 1st law has been developed to discuss the parabolic oxidation behaviour of HPSN. In spite of the several simplifications introduced, the model proves adequate to explain kinetic and thermodynamic aspects of oxidation of $(Y_2O_3$–$SiO_2)$-doped HPSN in terms of the amount and composition of the secondary phase. It also offers a chance to define optimum oxidation-resistant compositions and its use can be extended to other additive systems.

(iii) A schematic of the process included the following. At the beginning of the oxidation the concentration of yttria and other metal cations at the reaction interface equals C_{gb}, i.e. is higher than the equilibrium concentration C_{ri}.

This causes formation of intermediate compounds among Si_3N_4, yttria and other metal cations and possibly oxygen and makes the subsequent oxidation by atmosphere oxygen easier than the direct Si_3N_4–O_2 reaction which also occurs but at a very low rate. As a consequence a concentration gradient is established and diffusion of metal cations from the bulk of the material to the reaction interface occurs, which is suggested to govern oxidation. Diffusion of O^{-2}, or most probably N^{-3} as formerly proposed [14], may provide for the charge at the Si_3N_4/oxide reaction interface.

(iv) A procedure to evaluate E_a which accounts for the temperature dependence of some diffusion parameters in addition to D, gives results which should reflect more adequately the real processes operative during oxidation. A more detailed definition of the diffusion profiles is nevertheless required to substantiate the validity of the method.

References

1. A. J. KIEHLE, L. K. HEUNG, P. J. JELISSE and T. J. ROCKETT, *J. Amer. Ceram. Soc.* 58(1) (1975) 17.
2. S. C. SINGHAL, *J. Mater. Sci.* 11 (1976) 500.
3. D. CUBICIOTTI and K. H. LAU, *J. Electrochem. Soc.: Solid State Sci. Technol.* 126(10) (1979) 1724.
4. G. N. BABINI, A. BELLOSI and P. VINCENZINI, *Ceram. Int.* 7(3) (1981) 78.
5. G. N. BABINI, A. BELLOSI and P. VINCENZINI, *J. Amer. Ceram. Soc.* 64(10) (1981) 578.
6. S. C. SINGHAL, "Oxidation of Silicon Nitride and Related Materials", in NATO/ASI "Nitrogen Ceramics", edited by F. L. Riley (Noordhoff Publ.

Comp., London, 1976) p. 607.
7. G. Q. WEAVER and J. W. LUCEK, *Amer. Ceram. Soc. Bull.* 57(12) (1978) 1131.
8. G. N. BABINI, A. BELLOSI and P. VINCENZINI, *Ceram.* (3) (1981) 11.
9. C. L. QUACKENBUSH and J. T. SMITH, *Amer. Ceram. Soc. Bull.* 59(5) (1980) 533.
10. F. F. LANGE, S. C. SINGHAL and R. C. KUZNICKI, *J. Amer. Ceram. Soc.* 60(5–6) (1977) 249.
11. E. GUGEL, A. F. FICKEL and H. KESSEL, *Powder Met. Int.* 6 (1974) 136.
12. R. R. WILLS, J. A. CUNNINGHAM, J. M. WIMMER and R. W. STEWART, *J. Amer. Ceram. Soc.* 59(5–6) (1976) 269.
13. G. N. BABINI, A. BELLOSI and P. VINCENZINI, Oxidation Behaviour of Si_3N_4 Hot-Pressed with Various Sintering Aids, in "Science of Ceramics", Vol. 11, edited by R. Carlsson and S. Karlsson (Swedish Ceramic Society, Gothenburg, 1981) p. 291.
14. D. R. CLARKE and F. F. LANGE, *J. Amer. Ceram. Soc.* 63(9–10) (1980) 586.
15. D. CUBICIOTTI and K. H. LAU, *ibid.* 61(11–12) (1978) 512.
16. G. N. BABINI and P. VINCENZINI, "Oxidation Kinetics of Silicon Nitride", in "Progress in Nitrogen Ceramics", NATO/ASI Series, edited by F. L. Riley (Martinus Nijhoff Publishers, The Hague, Netherlands, 1983) p. 427.

Received 11 May
and accepted 26 July 1983